Next Generation Adaptive Optics System

KAON 686

NGAO Laser Launch Facility System Performance

Preliminary Design

May 20, 2010

VersionV1.2

Prepared By Thomas Stalcup, Jason Chin

REVISION HISTORY

Revision	Date	Author (s)	Reason for revision / remarks
1.0	Oct 19, 2009	All	Initial release
1.1	Nov 04, 2009	JC	Added KAON #
1.2	May 20, 2010	TS	Major updates for PDR

TABLE OF CONTENTS

1 INTRODUCTION

As part of the Next Generation Adaptive Optics System (NGAO), a Laser Launch Facility (LLF) System is needed to generate and propagate the laser beams. The LLF is made up of three subsystems: Beam Generation System (BGS), Beam Transport Optics (BTO); and the Switchyard (SYD). This document provides the preliminary design performance of the three subsystems and examines the overall performance of the LLF. A section will also described the diagnostics to support the LLF and associated subsytems.

2 SYSTEM PERFORMANCE

2.1 System Overview

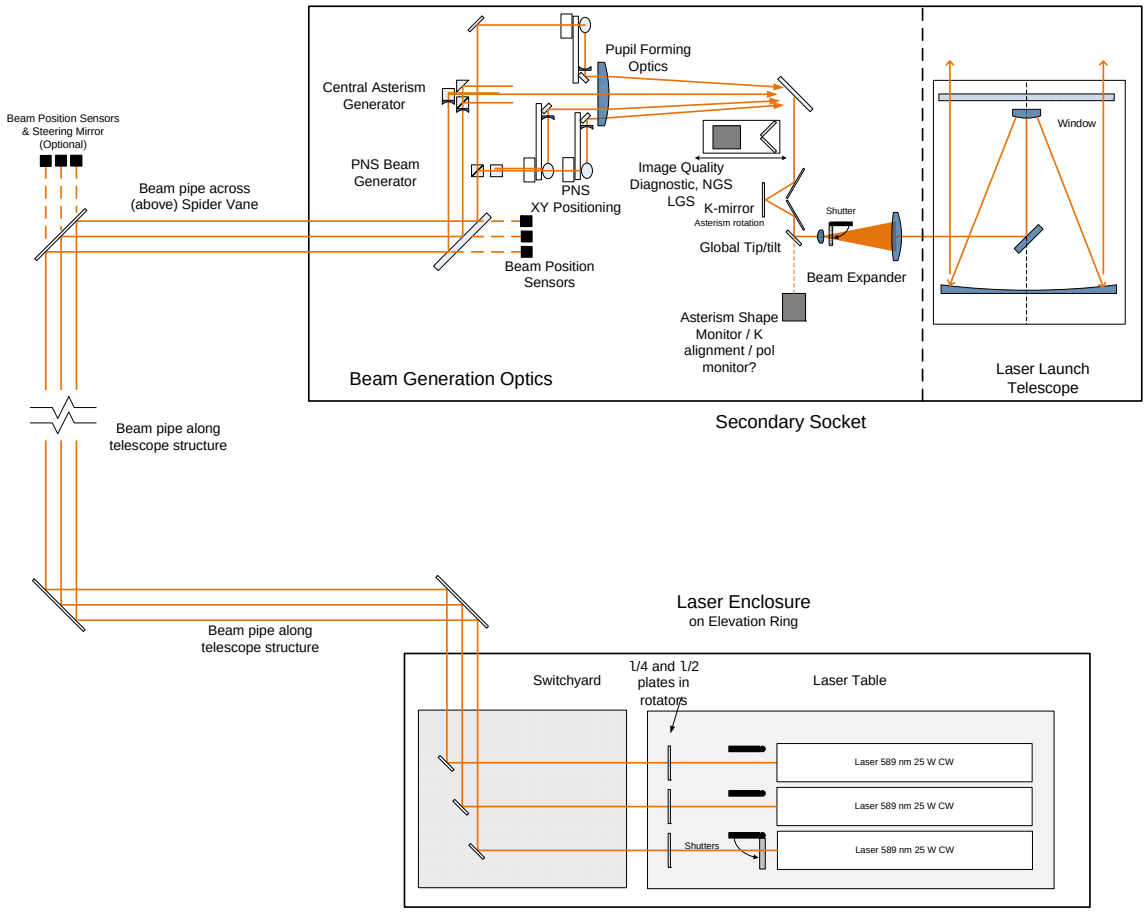

2.2 Throughput

Due to the number of surfaces in the LLF the system throughput has a strong sensitivity on the coating quality and surface cleanliness. As a result, good quality coatings are required along with procedures and design features to minimize the accumulation of dust and dirt on the surfaces. Periodic cleaning will be necessary so the coatings should also be hard to prevent damage. Ion Beam Sputtering (IBS) is one process that produces high performance coatings that are also very hard and insensitive to environmental factors such as humidity. Advanced Thin Films is one manufacturer that has demonstrated this type of coating for optics used in the K1 and Gemini laser projects. Their standard specification is 99.9% reflectance for mirrors and 0.1% reflectance for AR coatings. They claim a limit of 99.99% reflectance for mirrors and 100 ppm for AR coatings. Other manufacturers also offer similar coatings with similar characteristics. For the throughput analysis below, a slightly conservative value of 99.8% was used for both mirror and anti-reflection coatings.

Scattering loss due to accumulation of dust and dirt on the optics is, unfortunately, unavoidable. Since the BGS and the BTO are mounted on the telescope, it does not appear to be practical to only open them in a clean room environment so some accumulation is inevitable. To compensate for this, access for cleaning will be provided wherever possible and a cleaning schedule will be implemented based on the measured system throughput. For the throughput budget, a value of 1% scattering loss will be used for the BGS and

BTO components while a value of 0.5% will be used for the switchyard optics since the laser enclosure will provide a clean environment when the switchyard must be accessed. As a comparison, a surface with a cleanliness level 500 according to MIL STD 1246C has approximately 1% of its surface obscured. A horizontal surface in normal air in a Class 10,000 clean room will accumulate enough particles to reach level 500 in about one year. Vertical surfaces should accumulate at a rate about 1/10 that of a horizontal surface, and downward facing surfaces may be only 1/100 the horizontal value.[1]

In the table below, there are two overall values for the throughput, one for the "clean" state and one including the dust contribution. The total throughput will be monitored with power meters at the laser unit outputs and as close to the BGS output as possible. When the total throughput approaches the dusty value given below, the optics would need to be cleaned to restore the throughput to higher levels.

The throughput degradation for the given contamination levels is significant, with the dirty optics throughput at 62% versus the clean optics throughput at 86%. As the mechanical design is finalized, the per element dust and dirt contribution can be refined. The entire system will be enclosed with a light overpressure of filtered air, but there will still be some dust infiltration during maintenance and during the cleaning process itself. As a further dust reduction measure, some surfaces may be enclosed in a small, localized secondary enclosure or protective shrouds. One example would be a dust tight shroud between the two lenses in the beam expanders. This would allow reducing the dust scatter allowance for the inner two surfaces considerably below the standard value. The LTA is a sealed enclosure with no planned access so the dust contribution to its internal surfaces will be set to a low 0.1%.

		Element Name	Number of Surfaces	Reflection / Trans. per Surface	Dirt / scatter	Element Clean Total	Element Dirty Total
Switchyard	1	Laser Enc. Laser Mirror	1	99.80%	0.50%	99.80%	99.30%
	2	1/2 Wave Plate	2	99.80%	0.50%	99.60%	98.61%
	3	1/4 Wave Plate	2	99.80%	0.50%	99.60%	98.61%
	4	Beam Expander Telescope Lens 1 Front	1	99.80%	0.50%	99.80%	99.30%
	5	Beam Expander Telescope Lens 1 Back	1	99.80%	0.10%	99.80%	99.70%
	6	Beam Expander Telescope Lens 2 Front	1	99.80%	0.10%	99.80%	99.70%
	7	Beam Expander Telescope Lens 2 Back	1	99.80%	0.50%	99.80%	99.30%
	8	Laser Enc. Steering Mirror	1	99.80%	0.50%	99.80%	99.30%
	9	Laser Enclosure/BTO window inside	1	99.80%	0.50%	99.80%	99.30%
	10	Laser Enclosure/BTO window outside	1	99.80%	1.00%	99.80%	98.80%
Beam Transfer Optics	11	Top Ring Mirror 1	1	99.80%	1.00%	99.80%	98.80%
	12	Top Ring Mirror 2	1	99.80%	1.00%	99.80%	98.80%
	13	Sec. Socket Mirror 1	1	99.80%	1.00%	99.80%	98.80%
	14	Sec. Socket Mirror 2	1	99.80%	1.00%	99.80%	98.80%
	15	Sec. Socket Mirror 3	1	99.80%	1.00%	99.80%	98.80%
	16	Sec. Socket Mirror 4	1	99.80%	1.00%	99.80%	98.80%
Asterism Generator	17	Entrance Fold Mirror	1	99.80%	1.00%	99.80%	98.80%
	18	Fold Mirror	1	99.80%	1.00%	99.80%	98.80%
	19	Astr. Gen. B.S.	2	99.80%	1.00%	99.60%	97.62%
	20	Astr. Gen. Mirror	1	99.80%	1.00%	99.80%	98.80%
	21	Asterism Fold Mirror	1	99.80%	1.00%	99.80%	98.80%
	22	Negative Lens	2	99.80%	1.00%	99.60%	97.62%
	23	Pupil Imaging Lens	2	99.80%	1.00%	99.60%	97.62%
	24	Fold	1	99.80%	1.00%	99.80%	98.80%
	25	K Mirror Assembly	3	99.80%	1.00%	99.40%	96.45%
	26	Global TT mirror	1	99.80%	1.00%	99.80%	98.80%
	27	Beam Expander Telescope Lens 1 Front	1	99.80%	1.00%	99.80%	98.80%
	28	Beam Expander Telescope Lens 1 Back	1	99.80%	0.10%	99.80%	99.70%
	29	Beam Expander Telescope Lens 2 Front	1	99.80%	0.10%	99.80%	99.70%
	30	Beam Expander Telescope Lens 2 Back	1	99.80%	1.00%	99.80%	98.80%
	31	BTOB Fold	1	99.80%	1.00%	99.80%	98.80%
LTA	32	Launch Tel. Input Win. Surf 1	1	99.65%	1.00%	99.65%	98.65%
	33	Launch Tel. Input Win. Surf 2	1	99.65%	0.10%	99.65%	99.55%
	34	Launch Tel. Tertiary	1	99.65%	0.10%	99.65%	99.55%
	35	Launch Tel. Secondary	1	99.65%	0.10%	99.65%	99.55%
	36	Launch Tel. Primary	1	99.65%	0.10%	99.65%	99.55%
	37	Launch Tel. Output Win. Surf 1	1	99.65%	0.10%	99.65%	99.55%
	38	Launch Tel. Output Win. Surf 2	1	99.65%	0.35%	99.65%	99.30%
		LLT Secondary Obscuration				94.80%	
		Total				85.7%	62.3%

Table 1. Central asterism throughput.

		Element Name	Number of Surfaces	Reflection / Trans. per Surface	Dirt / scatter	Element Clean Total	Element Dirty Total
Switchyard	1	Laser Enc. Laser Mirror	1	99.80%	0.50%	99.80%	99.30%
	2	1/2 Wave Plate	2	99.80%	0.50%	99.60%	98.61%
	3	1/4 Wave Plate	2	99.80%	0.50%	99.60%	98.61%
	4	Beam Expander Telescope Lens 1 Front	1	99.80%	0.50%	99.80%	99.30%
	5	Beam Expander Telescope Lens 1 Back	1	99.80%	0.10%	99.80%	99.70%
	6	Beam Expander Telescope Lens 2 Front	1	99.80%	0.10%	99.80%	99.70%
	7	Beam Expander Telescope Lens 2 Back	1	99.80%	0.50%	99.80%	99.30%
	8	Laser Enc. Steering Mirror	1	99.80%	0.50%	99.80%	99.30%
	9	Laser Enclosure/BTO window inside	1	99.80%	0.50%	99.80%	99.30%
	10	Laser Enclosure/BTO window outside	1	99.80%	1.00%	99.80%	98.80%
Beam Transfer Optics	11	Top Ring Mirror 1	1	99.80%	1.00%	99.80%	98.80%
	12	Top Ring Mirror 2	1	99.80%	1.00%	99.80%	98.80%
	13	Sec. Socket Mirror 1	1	99.80%	1.00%	99.80%	98.80%
	14	Sec. Socket Mirror 2	1	99.80%	1.00%	99.80%	98.80%
	15	Sec. Socket Mirror 3	1	99.80%	1.00%	99.80%	98.80%
	16	Sec. Socket Mirror 4	1	99.80%	1.00%	99.80%	98.80%
Asterism Generator	17	Astr. Gen. B.S. 1	2	99.80%	1.00%	99.60%	97.62%
	18	Astr. Gen. B.S. 2	2	99.80%	1.00%	99.60%	97.62%
	19	Astr. Gen. Mirror 1	1	99.80%	1.00%	99.80%	98.80%
	20	Astr. Gen. Mirror 2	1	99.80%	1.00%	99.80%	98.80%
	21	Astr. Gen. Mirror 3	1	99.80%	1.00%	99.80%	98.80%
	22	Negative Lens	2	99.80%	1.00%	99.60%	97.62%
	23	Pupil Imaging Lens	2	99.80%	1.00%	99.60%	97.62%
	24	Fold	1	99.80%	1.00%	99.80%	98.80%
	25	K Mirror Assembly	3	99.80%	1.00%	99.40%	96.45%
	26	Global TT mirror	1	99.80%	1.00%	99.80%	98.80%
	27	Beam Expander Telescope Lens 1 Front	1	99.80%	1.00%	99.80%	98.80%
	28	Beam Expander Telescope Lens 1 Back	1	99.80%	0.10%	99.80%	99.70%
	29	Beam Expander Telescope Lens 2 Front	1	99.80%	0.10%	99.80%	99.70%
	30	Beam Expander Telescope Lens 2 Back	1	99.80%	1.00%	99.80%	98.80%
	31	BTOB Fold	1	99.80%	1.00%	99.80%	98.80%
LTA	32	Launch Tel. Input Win. Surf 1	1	99.65%	1.00%	99.65%	98.65%
	33	Launch Tel. Input Win. Surf 2	1	99.65%	0.10%	99.65%	99.55%
	34	Launch Tel. Tertiary	1	99.65%	0.10%	99.65%	99.55%
	35	Launch Tel. Secondary	1	99.65%	0.10%	99.65%	99.55%
	36	Launch Tel. Primary	1	99.65%	0.10%	99.65%	99.55%
	37	Launch Tel. Output Win. Surf 1	1	99.65%	0.10%	99.65%	99.55%
	38	Launch Tel. Output Win. Surf 2	1	99.65%	0.35%	99.65%	99.30%
		LLT Secondary Obscuration				94.80%	
		Total				85.6%	61.6%

Table 2. Patrolling asterism throughput.

2.3 Projected Spot size

The critical performance metric for the laser launch facility is the projected spot size at the sodium layer. A fundamental design choice is the Gaussian beam parameters of the output beam. This decision is a balance between a smaller output beam that minimizes the spot degradation due to atmospheric turbulence and a larger output beam minimizes the spot size due to diffraction effects.

The projection optical system is based on the same system that was used for the recent Keck 1 laser upgrade, which has an exit aperture diameter of 0.5 m and a nominal output Gaussian waist diameter of 0.36 m. Given these parameters, the optical properties of Gaussian beams define the minimum waist size for a range of projected waist locations. This relationship is shown in Figure 1. Note that there is a maximum altitude at which the beam waist can be placed at, and that below that maximum altitude there are two possible solutions. The upper, dashed branch of the graph corresponds to a larger waist size and thus a beam that diverges more slowly, while the lower branch corresponds to the solution with the smaller waist size and faster divergence.

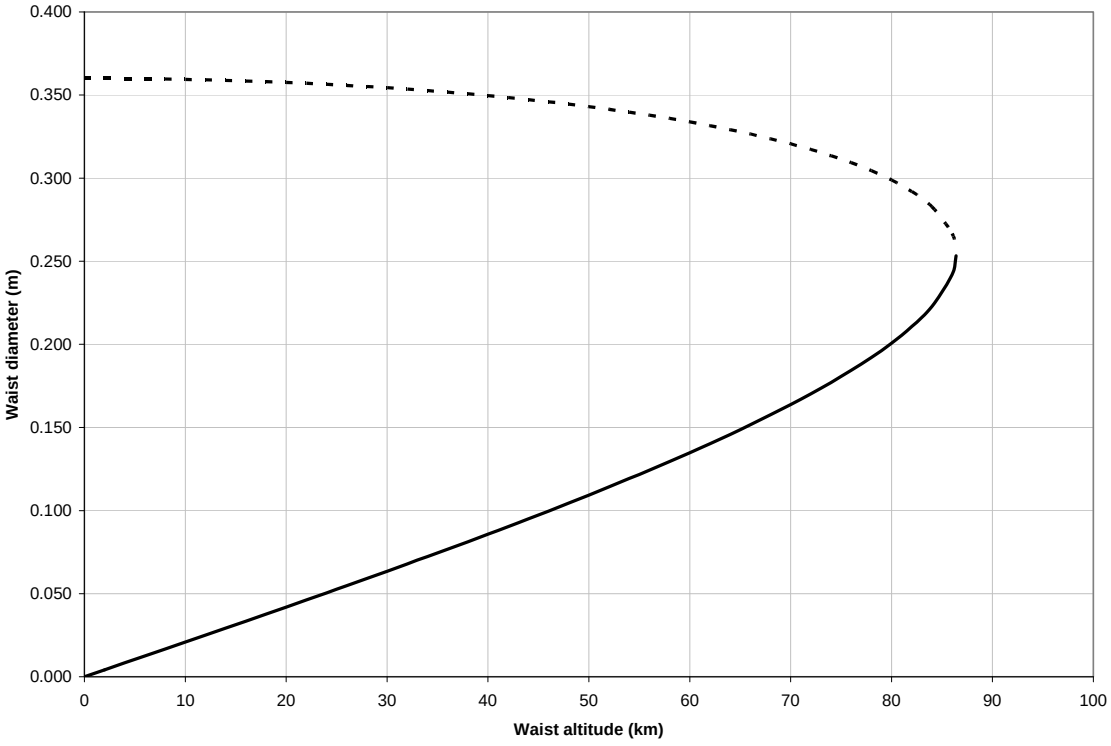

Figure 1. Projected gaussian beam waist size vs. altitude. The solid and dashed lines correspond to the two possible spot sizes given a 360 mm diameter output beam.

Given a projected waist size and location, the Gaussian beam propagation relationships can be used to find the beam size at the sodium layer. Figure 2 shows the 50% encircled energy diameter spot size for two different ranges to the sodium layer as a function of the altitude of the projected beam waist. The two ranges are 85 km and 170 km, which correspond to telescope zenith angles of 0 and 60 degrees. A projected waist altitude of approximately 78 km is a good compromise for spot sizes at all elevations, although if the projected waist altitude is variable and tracks the telescope elevation the aberration free spot size can be almost 10 percent smaller.

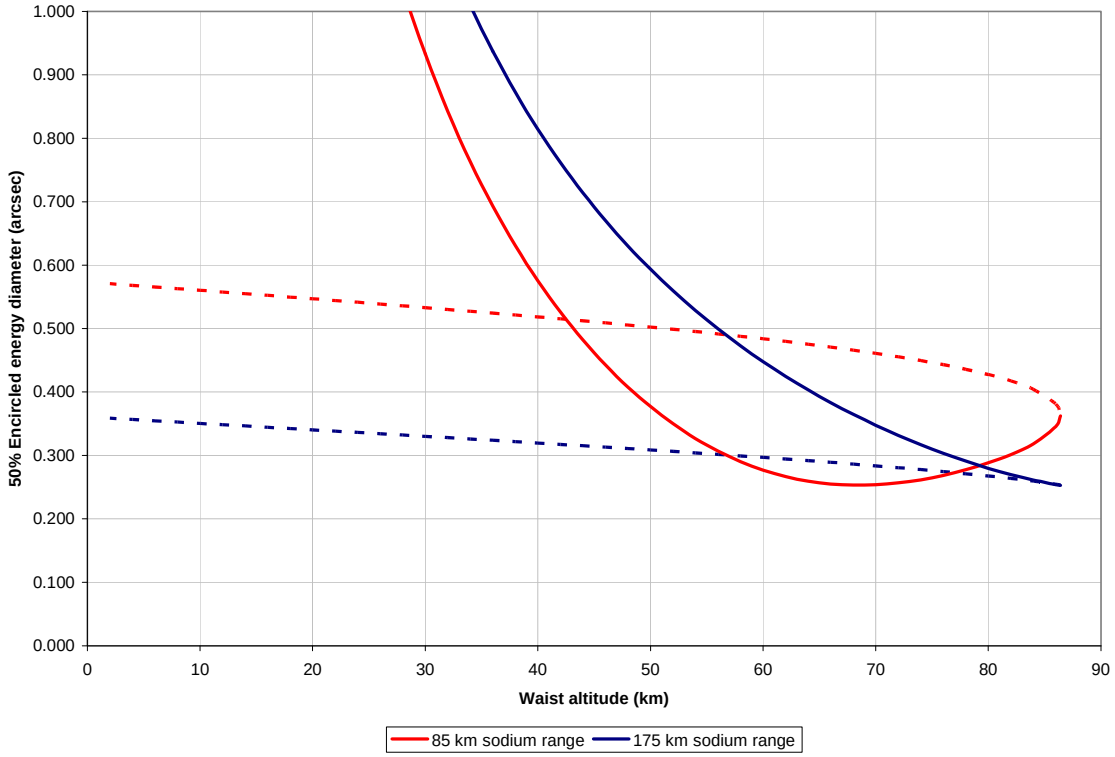

Figure 2. 50% encircled energy spot size in arcseconds vs. waist altitude. The dashed portion of each plotted line corresponds to the larger waist, dashed solution from Figure 1.

Aberration in the projected beam will tend to enlarge the projected spot. If we assume that the optical design of the beam projector is well-corrected, the major wavefront error contribution will come from random figure errors on the optics. To model this effect, a phase screen simulating a random wavefront error was generated by combining random amplitudes of zernike polynomials number 5 through 210. This phase screen was then applied to a perfect Gaussian beam and the resulting encircled energy diameters found using the physical optics propagation feature of Zemax. The amplitude of the phase screen was scaled to produce a range of rms wavefront errors to show the dependence between the encircled energy diameter and the rms wavefront error. This process was repeated for 30 different phase screens. Figure 3 shows an example phase screen and projected spot image and Figure 4 shows the results for all 30 phase screens. Each line in Figure 4 is the result from varying the amplitude of a single phase screen to produce various wavefront errors.

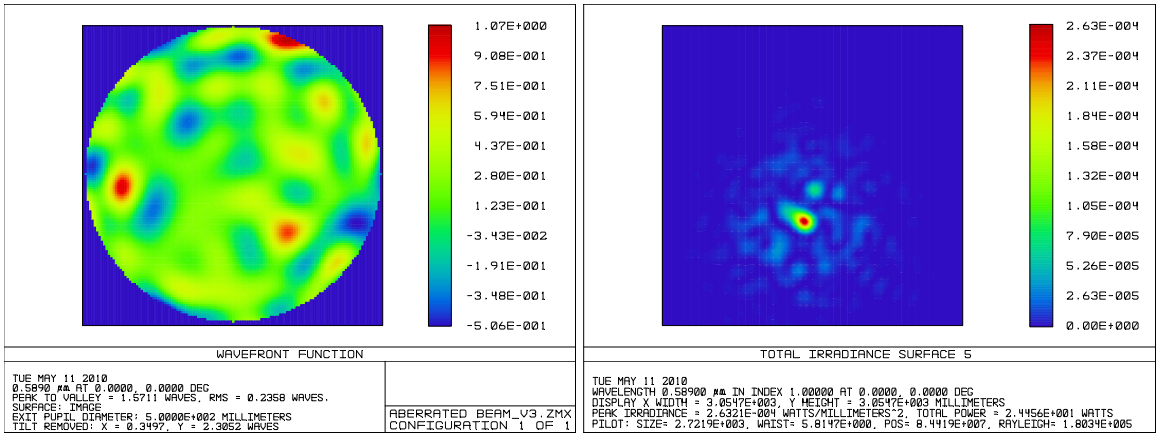

Figure 3. Example wavefront error and projected spot pattern from laser projector wavefront error testing.

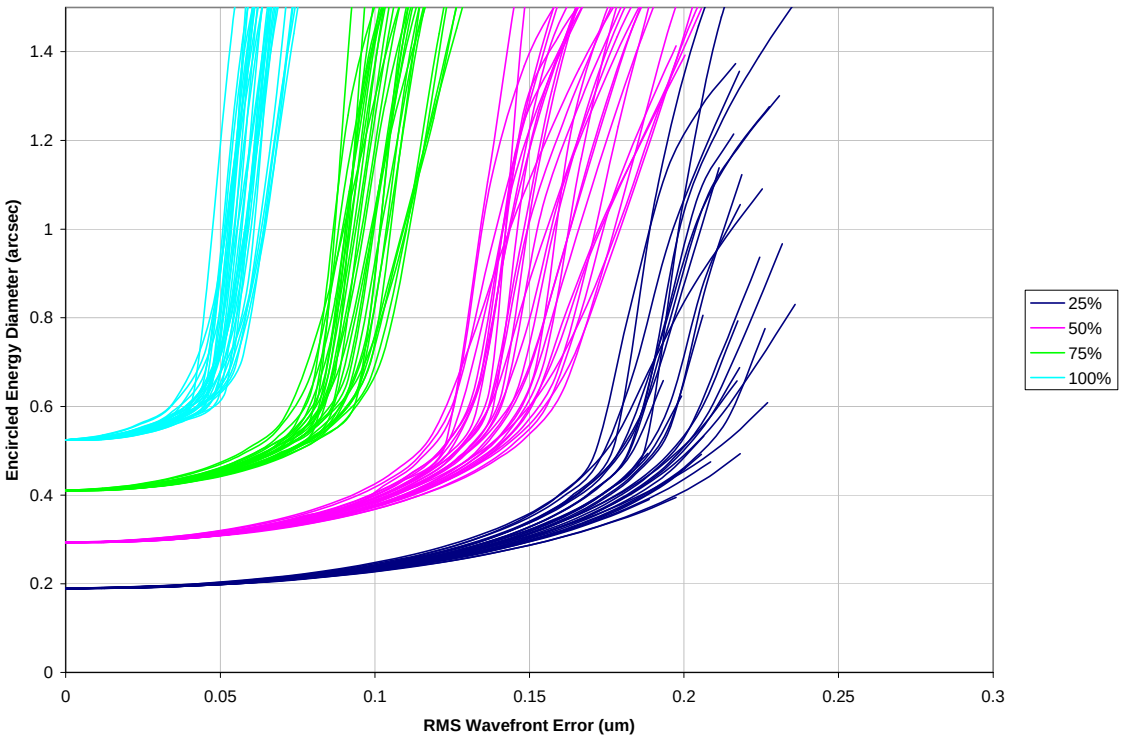

Figure 4. Projected spot encircled energy vs. projection optics wavefront error.

The shape of the curves in Figure 4 is due to the fact that the image can be modelled as a combination of the unaberrated Gaussian spot and a scattered halo from the phase aberrations. As the amplitude of the wavefront phase aberrations increase, more light is diffracted from the core into the halo. For small aberrations, there is much more light in the core than in the halo so the encircled energy is not affected much. This holds true until the energy in the core falls close to the encircled energy threshold in question,

and as the aberration is increased further the encircled energy diameter rapidly grows to include much of the halo.

Although the requirements specify the spot size at the sodium layer without atmosphere, as a check, Chris Neyman ran simulations of the up-beam path that included the atmosphere. These were done using the Mauna Kea ridge turbulence model for median seeing conditions. In each case, 1000 independent atmospheric phase screens were calculated and the resulting spot determined. Figure 5 shows data for different projected waist locations in the case of perfect projection optics.

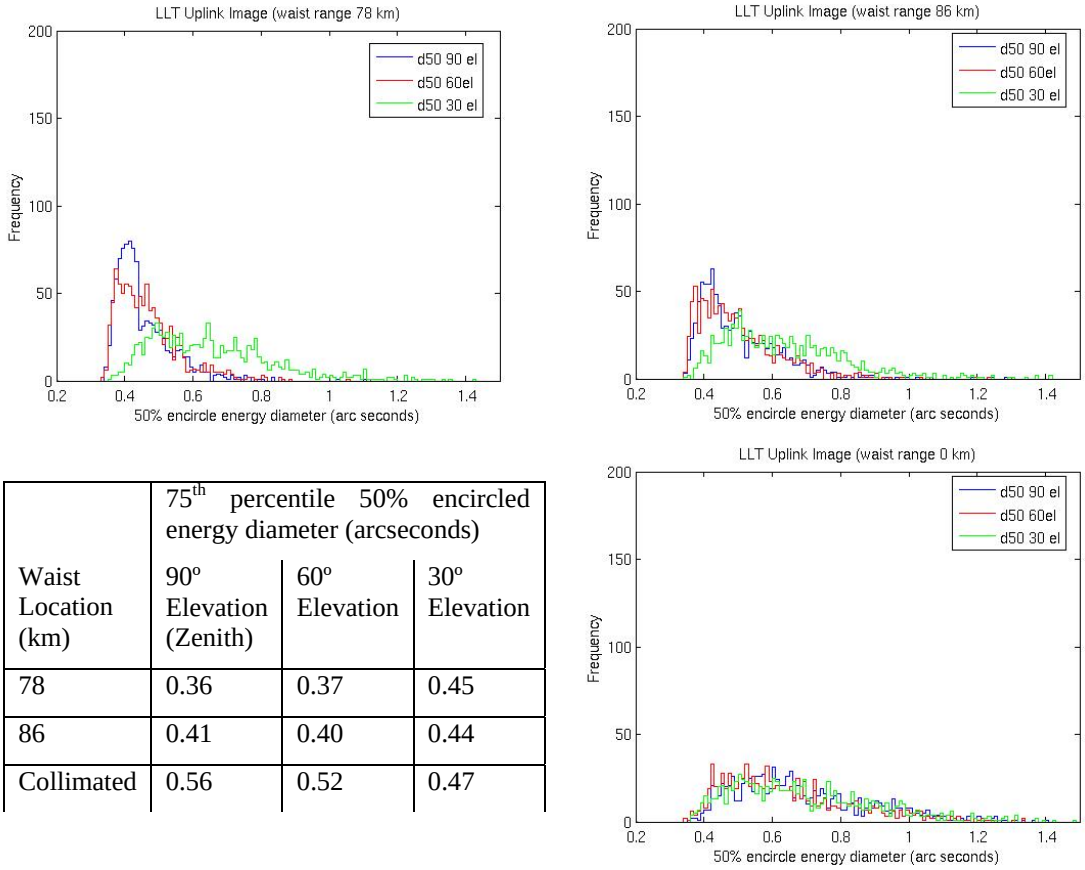

Waist Location (km)	75th percentile 50% encircled energy diameter (arcseconds)		
	90º Elevation (Zenith)	60º Elevation	30º Elevation
78	0.36	0.37	0.45
86	0.41	0.40	0.44
Collimated	0.56	0.52	0.47

Figure 5. Uplink spot 50% encircled energy diameter statistics at different telescope elevations for beam waists at different ranges. Clockwise from upper left: 78 km, 86 km, collimated (0 km). The table contains the 75th percentile values for the 50% encircled energy diameter distributions.

These results show that at high elevations, the spot size for the waist at 78 km is about 10% smaller than that for the waist at 86 km. At low elevations, however, there is very little difference between the two cases. This would seem to indicate that it is not worthwhile to have the beam projector focus track elevation, although it would be useful to include a test case with the optimum zenith case spot size waist at 68 km to verify this.

A final set of simulations done by Chris Neyman was to model the effects of beam projector wavefront error. This was done in a similar manner with a single waist range of 86 km and four different amounts of random wavefront error modelled as the sum of random amplitude Zernike polynomials number 4 through 22. The actual distributions appear in Figure 6, and Figure 7 plots the 75th percentile of the 50% encircled energy diameter distributions.

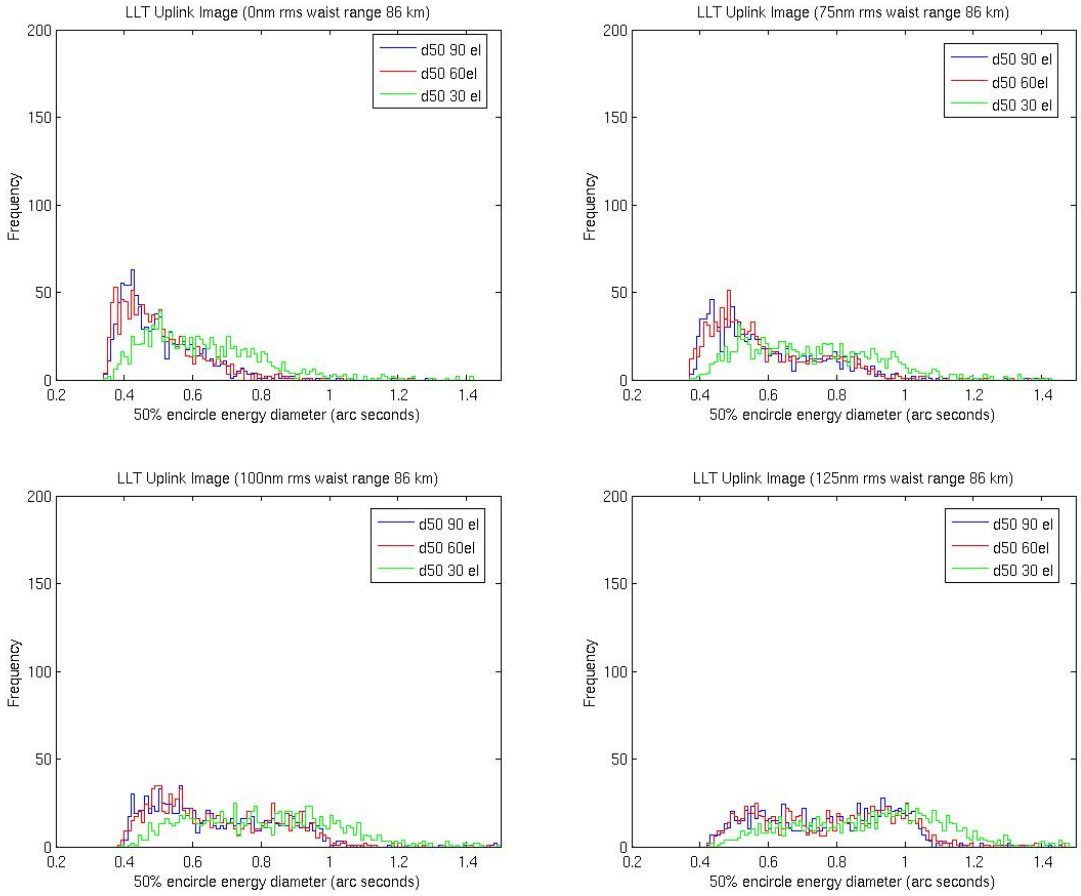

Figure 6. 50% encircled energy diameters at three elevations angles for different amounts of beam projector wavefront error, 0, 75, 125, 100 nm rms clockwise from upper left.

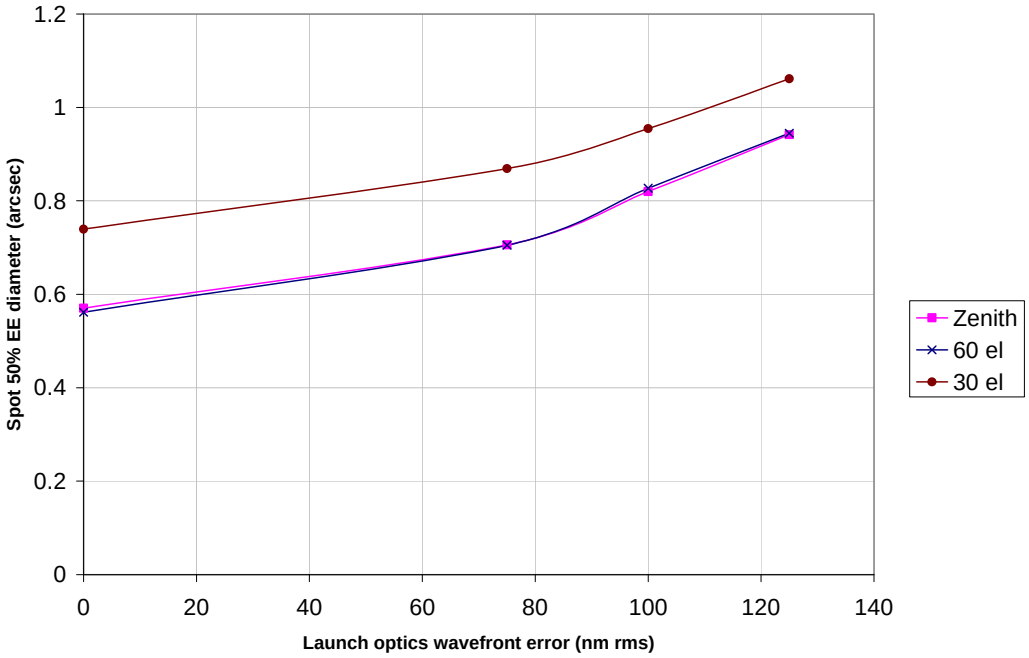

Figure 7. 75th percentile of the 50% encircled energy spot diameter as a function of launch optics wavefront error.

Based on all of the above data, a total system wavefront error allowance of 110 nm rms seems reasonable, and should deliver a system that produces a spot with a 0.45 arcsecond 50% encircled energy diameter in the absence of atmospheric turbulence. Including the atmospheric terms should result in a spot with a 50% encircled energy diameter of approximately 0.9 arcseconds. Since the specification for the maximum wavefront error from the laser is 70 nm rms, the launch optics can contribute 85 nm rms. Due to the number of surfaces in the laser launch facility this results in a tight figure error specification per surface. Table 3 and Table 4 have a complete list of the elements in the system and their corresponding wavefront error specification. Mirrors and spherical lenses are allocated 7 nm rms while beamsplitters and aspheric lenses are allocated slightly more at 10 nm rms. The values for the LTA elements come from its requirements document. Note that these specifications apply over an area the size of the laser beam footprint on each optic, so the rms over the entire surface is allowed to be larger. To specify this properly the structure function of the error should be taken into account, and this will be done prior to producing the fabrication drawings for the optical elements. As a point of reference, a quote of $720 for an uncoated 100 mm diameter mirror with a 6.3 nm rms figure error overall specification was recently obtained from Nu-Tek Precision Optical Corporation. This is slightly larger than the fold mirrors that will be required for the beam train. The cost for coating is $1500 for a lot that can be comprised of several mirrors of this size.

The system wavefront error specification is an area that should be revisited during the detailed design phase. A specification of 110 nm rms total is very close to a knee in both the spot size and cost curves. While the specification for the laser wavefront error is 70 nm rms, currently the prototype is performing closer to 35 nm rms. If the delivered unit has similar performance, this alone would drop the overall wavefront error to 90 nm rms. It is possible to significantly reduce the wavefront error in the BGS beam expander design, however it would mean making more surfaces aspheric which will increase the cost. Further modelling of the spot using real atmospheric phase screens and including all aberrations in both the up and down path would give more confidence in the calculated spot sizes and the real spot as seen by the wavefront sensor.

		Element Name	Number of Surfaces	WFE per Surface (nm rms)	WFE per Element (nm rms)
Switchyard	1	Laser Enc. Laser Mirror	1	7.0	7.0
	2	1/2 Wave Plate	2	10.0	14.1
	3	1/4 Wave Plate	2	10.0	14.1
	4	Beam Expander Telescope Lens 1	2	7.0	9.9
	6	Beam Expander Telescope Lens 2	2	7.0	9.9
	7	Beam Expander Telescope Design	1	5.0	5.0
	8	Laser Enc. Steering Mirror	1	7.0	7.0
	10	Laser Enclosure/BTO window	2	7.0	9.9
Beam Transfer Optics	11	Top Ring Mirror 1	1	7.0	7.0
	12	Top Ring Mirror 2	1	7.0	7.0
	13	Sec. Socket Mirror 1	1	7.0	7.0
	14	Sec. Socket Mirror 2	1	7.0	7.0
	15	Sec. Socket Mirror 3	1	7.0	7.0
	16	Sec. Socket Mirror 4	1	7.0	7.0
Asterism Generator	17	Entrance Fold Mirror	1	7.0	7.0
	18	Fold Mirror	1	7.0	7.0
	19	Astr. Gen. B.S.	2	10.0	14.1
	20	Astr. Gen. Mirror	1	7.0	7.0
	21	Asterism Fold Mirror	1	7.0	7.0
	22	Negative Lens	2	7.0	9.9
	23	Pupil Imaging Lens	2	7.0	9.9
	24	Fold	1	7.0	7.0
	25	K Mirror Assembly	3	7.0	12.1
	26	Global TT mirror	1	7.0	7.0
	27	Beam Expander Telescope Lens 1	2	10.0	14.1
	29	Beam Expander Telescope Lens 2	2	10.0	14.1
	30	Beam Expander Telescope Design	1	19.0	19.0
	31	BTOB Fold	1	7.0	7.0
LTA	32	Launch Tel. Input Win. Surf 1	2	6.0	8.5
	34	Launch Tel. Tertiary	1	6.0	6.0
	35	Launch Tel. Secondary	1	35.0	35.0
	36	Launch Tel. Primary	1	45.0	45.0
	37	Launch Tel. Output Win. Surf 1	2	11.0	15.6
		Total			79.7

Table 3. Wavefront error for central laser asterism.

		Element Name	Number of Surfaces	WFE per Surface (nm rms)	WFE per Element (nm rms)
Switchyard	1	Laser Enc. Laser Mirror	1	7.0	7.0
	2	1/2 Wave Plate	2	10.0	14.1
	3	1/4 Wave Plate	2	10.0	14.1
	4	Beam Expander Telescope Lens 1	2	7.0	9.9
	5	Beam Expander Telescope Lens 2	2	7.0	9.9
	6	Beam Expander Telescope Design	1	5.0	5.0
	7	Laser Enc. Steering Mirror	1	7.0	7.0
	8	Laser Enclosure/BTO window	2	7.0	9.9
Beam Transfer Optics	9	Top Ring Mirror 1	1	7.0	7.0
	10	Top Ring Mirror 2	1	7.0	7.0
	11	Sec. Socket Mirror 1	1	7.0	7.0
	12	Sec. Socket Mirror 2	1	7.0	7.0
	13	Sec. Socket Mirror 3	1	7.0	7.0
	14	Sec. Socket Mirror 4	1	7.0	7.0
Asterism Generator	15	Astr. Gen. B.S. 1	2	10.0	14.1
	16	Astr. Gen. B.S. 2	2	10.0	14.1
	17	Astr. Gen. Mirror 1	1	7.0	7.0
	18	Astr. Gen. Mirror 2	1	7.0	7.0
	19	Astr. Gen. Mirror 3	1	7.0	7.0
	20	Negative Lens	2	7.0	9.9
	21	Pupil Imaging Lens	2	7.0	9.9
	22	Fold	1	7.0	7.0
	23	K Mirror Assembly	3	7.0	12.1
	24	Global TT mirror	1	7.0	7.0
	25	Beam Expander Telescope Lens 1	2	10.0	14.1
	26	Beam Expander Telescope Lens 2	2	10.0	14.1
	27	Beam Expander Telescope Design	1	33.5	33.5
	28	BTOB Fold	1	7.0	7.0
LTA	29	Launch Tel. Input Win. Surf 1	2	6.0	8.5
	30	Launch Tel. Tertiary	1	6.0	6.0
	31	Launch Tel. Secondary	1	35.0	35.0
	32	Launch Tel. Primary	1	45.0	45.0
	33	Launch Tel. Output Win. Surf 1	2	11.0	15.6
		Total			85.3

Table 4. Wavefront error for patrolling laser asterism.

2.4 Focus Error

Maintaining proper focus of the projected laser spot is important to the overall system performance. The only accurate method to obtain information about the quality of the laser focus at the sodium layer is to vary the beam projector focus and measure the change in spot size. This process can take several minutes due to the need to sample a few different focus positions and to average out seeing effects. This can be done as a part of the initial nightly calibrations, however it is undesirable to do this during the night as it will decrease the observing efficiency.

Much of the laser launch facility has slow, nearly collimated beams which are not very sensitive to focus errors. There are a few places that are sensitive to focus variations, however, such as the beam expanders and the LLT. To explore how sensitive the system is to focus variations, the expected length change between various parts of the system was calculated based on the coefficient of thermal expansion for the material it is made of and assuming a 10ºC temperature change. This length change was applied one surface at a time to the zemax model and the resulting 50% encircled energy spot size recorded. The resulting data is tabulated in Table 5, and is useful to identify potential problem areas for further study. During the detailed design phase, real numbers from FEA analysis will be used to generate a more detailed model of the effects of temperature change.

			Length (mm)		50% encircled energy diameter (arcsec)	
Element	**Material**	**CTE (ppm/C)**	**Nominal**	**Delta 10C**	**85 km**	**170 km**
Nominal spot size					0.274	0.293
Laser head						
	400 Stainless	10	110	0.011	0.274	0.293
Beam expander lens 1						
	400 Stainless	10	300	0.030	0.275	0.284
Beam expander lens 2						
	Mild Steel	8	22646	1.812	0.274	0.293
Path length change due to patrolling xy stage motion	air		0	53.750	0.274	0.289
Negative lens						
	400 Stainless	10	50	0.005	0.274	0.293
Pupil forming lens						
	400 Stainless	10	780	0.078	0.274	0.293
Beam expander lens 1						
	Invar 36	1.6	220	0.004	0.285	0.281
Beam expander lens 2						
	400 Stainless	10	95	0.010	0.274	0.293
LLT entrance						
	CFRP	1	630	0.006	0.274	0.293
LLT secondary						
	CFRP	1	464	0.005	**0.795**	**1.04**
LLT primary						

Table 5. Resultant spot size due to focus errors.

The two worst offenders were the BGS beam expander and the LLT itself. Based on this, the material for the BGS beam expander mount was chosen to be invar, which results in a reasonably small change in the spot size. If this spot size change proves to be unacceptable during the detailed design phase, a focus vs. temperature model can be used to adjust this spacing. The BGS beam expander spacing will be motorized regardless to allow control of the overall beam projector focus.

The temperature effects in the LLT, however, are unacceptable even with the low expansion coefficient of its carbon fiber support structure if no further methods are used to control it. This was known prior to writing the requirements for the LLT and the need for further thermal stabilization was included. The contract for the LLT has been awarded, and the contractor is currently planning to incorporate a compensating material in the thermal stack-up between the primary and secondary to result in a net near-zero thermal expansion coefficient for the design as a whole. Temperature sensors are also included in the LLT design, and will be used to characterize the focus vs. temperature behaviour of the LLT prior to delivery. This will allow compensation of the focus error with the motorized action of the BGS beam expander.

The only non-thermal focus error expected in the system is the path length change due to the x-y motion of the patrolling laser asterism generator. Beacons at the edge of the field will experience a path length change of up to 54 mm relative to the center of the field. As shown in Table 5, this results in a negligible change in the spot size on sky.

2.5 Pointing Error

There are a few different possible meanings to "pointing error" when talking about the laser projection system, however the most important is related to FR-2353, blind pointing (startup) and FR-1952, blind pointing. FR-2353 applies at the beginning of the night to the initial laser propagation, prior to any update of the pointing model. FR-1952 applies at any other time, after the laser pointing model has been updated by any measurements made in the beginning of the night.

Pointing errors can be grouped into two main classes, repeatable errors and non-repeatable errors. Repeatable errors are a function of some combination of flexure, temperature, or the position of some element. Since they are repeatable, they can be corrected with an open-loop lookup table and only the error in the model should contribute to the total on-sky pointing error. Non-repeatable errors are due to hysteresis, mechanical stick/slip action, actuator homing errors, or errors in position feedback loops. These can only be corrected if there is some method to sense the resulting error.

Pointing error control in the LGSF is based on a combination of open- and closed-loop corrections. The open-loop corrections keep the beacons in approximately the correct location and within the dynamic range of the closed loop systems which then correct for any residual error. There are two closed-loop systems, one that corrects errors between the laser heads and the BGS entrance, and one that allows fine correction of the location of all seven beacons prior to projection.

The first closed loop system uses position sensors at the entrance to the BGS to determine the residual error from the laser heads through the BTO. This measured position error is then corrected by a high precision steering mirror in the laser switchyard. This stabilizes the input beam to the BGS and corrects for most of the error from the main telescope, laser switchyard and laser heads. Since there is only one steering mirror there is some small residual error from the resulting angle equivalent to a maximum of 0.27 arcseconds on sky. This is easily corrected by the second closed loop system.

The second closed loop pointing error correction system uses a camera that images the leakage from the final fold mirror that sends the light into the LLT. This asterism camera covers the entire field and provides a final check on the laser alignment. Since it uses the leakage from a mirror, it is always available without any throughput penalty and can be used to continuously track and correct any errors in the laser pointing. A shutter between this fold mirror and the LLT allows checking the BGS setup while acquiring a new target without actually propagating the laser to the sky. This is a critical feature of the BGS to reduce the blind pointing error, and effectively negates the effect of any flexure or pointing errors in the beam train prior to it. The plate scale for the asterism camera will be approximately 150 milliarcseconds/pixel, so if the spot centroid is measured to half a pixel the measurement error will be 75 milliarcseconds at the camera. There are a few different elements used to correct these measured errors. A position error of the entire central asterism is corrected with the global tip/tilt mirror, while a rotational error is corrected with the K-mirror. Although the central asterism generator assembly is fixed and has no internal adjustments, the position of the two input beams can be adjusted by applying a small offset to the position control loop for these two lasers at the BGS entrance. Since each laser is split to create two of the four beams of the central asterism, this allows adjustment of the relative position of the two pairs of beams that make up the central asterism. Any error in the patrolling guidestars is corrected with offsets to the x-y stages that position them.

After the asterism camera, however, there are a few opportunities where pointing error can be introduced. The asterism camera assembly and the fold mirror mount must be very stiff as any flexure will contribute an un-sensed error. Another error source is flexure inside the LLT itself. The LLT is specified to be a stiff assembly, and since it should have very little hysteresis or other non-repeatable error a good flexure model will correct for its pointing error. The LLT mechanical design is currently in progress and a preliminary design review is scheduled for July 13th, 2010. More details of the expected flexure will be available then.

The largest source for pointing error is flexure in the main telescope itself that creates a tilt in the entire top end of the telescope. This is currently seen as a secondary mirror tilt term that is observed during pointing and phasing runs. The primary effect of this for the main telescope is a small pointing offset which is corrected in the pointing model. The laser projector, however, will not benefit from this correction and may have to point even further off axis to compensate for the combined effect of the main telescope pointing model and the top end flexure. On Keck 2 the amplitude of this tilt is about 20 arcseconds between zenith and horizon. The current Keck 2 laser system flexure model results in proper pointing most of the time, but occasionally has pointing errors up to 5-7 arcseconds. It is not clear if this is a problem with the flexure model for the main telescope or if it comes from elements within the laser system itself. The source of this error is currently being investigated.

After propagating to the sky, the laser wavefront sensors on the AO bench provide feedback to correct the beacon positioning using the same adjustments that were used to correct for the errors measured by the asterism camera. The positioning error is determined by the resolution of the various stages in the BGS, which is 15 milliarcseconds for the patrolling guidestar position and 5 milliarcseconds for the central asterism.

As with the focus error, a detailed pointing error analysis will be produced during the detailed design phase based on the results of FEA analysis of the mechanical design.

2.6 Polarization Control

The LLF is specified to be circularly polarized with an ellipticity less than 10%. The laser output will be linearly polarized. This linear polarization will be converted to circular polarization by using a quarter-wave plate. Unfortunately, the polarization state of the beam will change slightly after every reflection due to phase shifts in the mirror coatings so it is not possible to simply produce circular polarization in the laser enclosure and transmit it through the rest of the LLF.

It is possible, however, to control the polarization state of the beams in the laser enclosure such that the initial polarization state compensates for the polarization change in the rest of the LLF resulting in a circularly polarized output. This is complicated, however, by the fact that in the BGS the output from each laser is split into multiple beams. If the polarization shifts experienced by all of the beams created from a single laser are not identical, they can not be compensated by a single waveplate at the laser head. The polarization properties of dielectric mirror coatings have an angular dependence so any element where there is a range of angles for the different beams must be carefully designed.

Adding an extra initial layer of high index material on top of a typical quarter-wave stack high reflectance coating allows tuning of the differential phase shift by adjusting its thickness.[2] This was tested in Zemax by applying such a coating to the K-mirror elements and manually tuning the thickness of the initial high index layer. The coating for the first and last mirrors in the assembly was $0.96H(LH)^{10}$, and the coating for the second mirror in the assembly was $1.17H(LH)^{10}$. The range of field angles used in this model is ± 2.7 degrees, which matches those present between the pupil forming lens and the BGS beam expander. Figure 8 shows the phase shift for the coating on the first mirror in the assembly that has a nominal angle of incidence of 56.5 degrees. Note that while the differential phase shift for s- and p-polarizations is not zero, it is constant over the field. The result of this is that a circularly polarized input beam is elliptically polarized after reflection, but all beams over this range of field angles have the same elliptical polarization. Because all of these beams are identical, the elliptical output can be corrected by properly adjusting the input polarization. The overall output after all three reflections in the K-mirror had a differential phase shift of 5.6 degrees and an overall transmission of 99.68%.

During the detailed design phase, this coating design will be finalized with a coating manufacturer and the overall system polarization effects calculated.

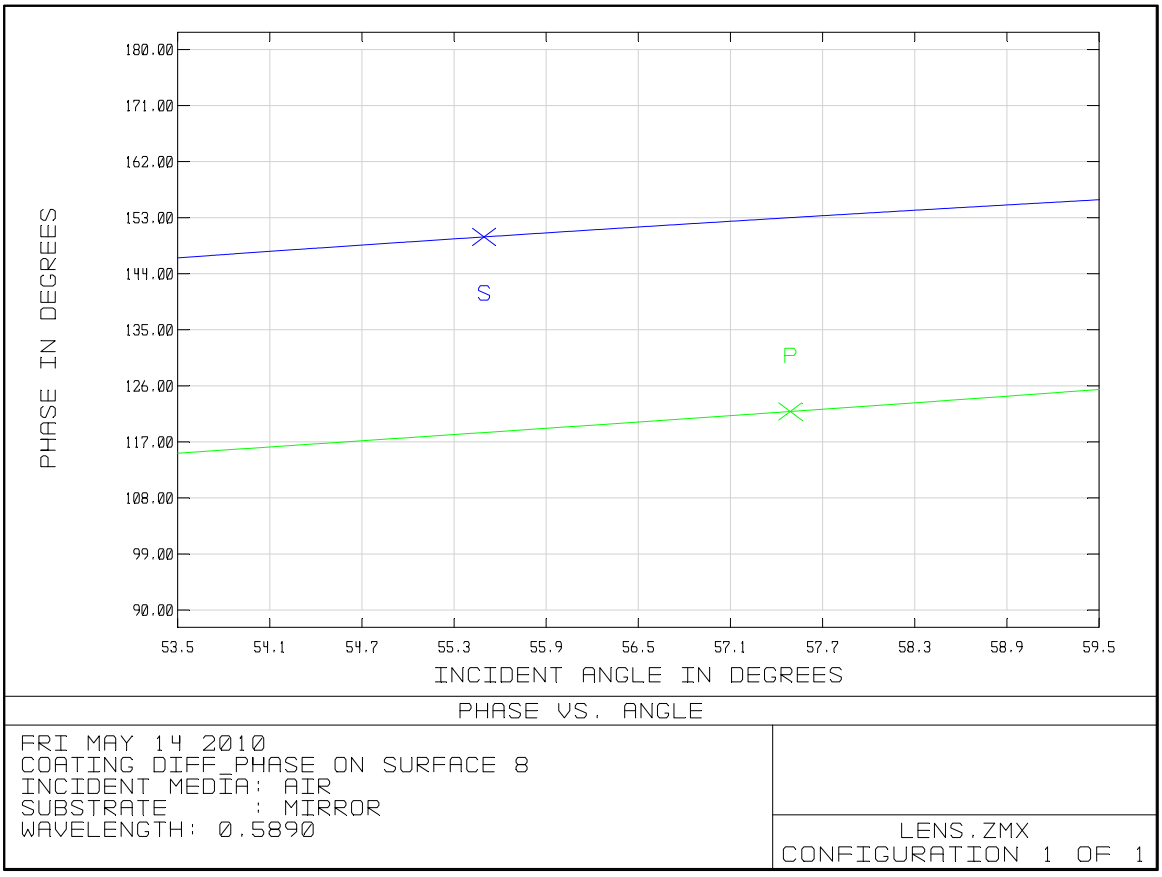

Figure 8: Polarization dependent phase shift vs. angle for mirror coating

3 DIAGNOSTICS

The laser units for NGAO are highly engineered, stable, semi-commercial units. As such, their output is expected to be high quality and very consistent, with very little user intervention necessary or even possible. Because of this, the need for real-time diagnostics is greatly reduced. In comparison, a previous generation laser, such as the Keck 2 dye laser, requires constant supervision and manual optimization so real-time diagnostics are essential for efficient operation. Table 6 shows the laser beam related diagnostics in the Laser Guide Star Facility. Environmental and internal subsystem type diagnostics are not represented here.

Diagnostic Measurement	Subsystem	Real Time / Non Real Time
Laser Wavelength	Laser	Real Time
Laser Output Power	Laser	Real Time
Laser Output Spectrum	Laser	Real Time
M^2	Switchyard	Non-real time
Wavefront Measurement	Switchyard	Non-real time
Beam Profile	Switchyard	Non-real time
Encircle Energy	Switchyard	Non-real time
Polarization	Switchyard	Non-real time
Laser Power	Switchyard	Non-real time
Beam/Asterism Position	BGS	Real Time
Laser Power	BGS	Real Time

Table 6: LGSF Laser Related Diagnostics

Because of the expected stability of the laser, the only real-time diagnostics included are output power and beam position for the Laser Launch Facility. The position sensors at the BGS input provide both position and total power, and will correct for any pointing drift from the laser head in addition to that from telescope flexure. The asterism camera can also be used as a real-time power measurement device.

The off-line diagnostics are all located at the exit of the switchyard in the laser enclosure. A mirror on a translation stage is used to send any of the three laser beams into a variety of diagnostic hardware listed below. Note that it is possible to implement these as real time diagnostics by replacing this mirror with a beam sampling element.

Wavefront sensor and M^2 montior. This is a standard Shack-Hartmann based wavefront sensor that will also calculate the M^2 quality factor for the laser. In addition to M^2, it will provide the laser wavefront error, beam profile, and encircled energy.

Polarimeter. This will be a standard polarimeter unit to measure the polarization state of the laser outputs.

Beam dump power monitor or beam profiler. The current plan is for this to be an accurate combination beam dump and power monitor. If the resolution of the beam profile or the encircled energy obtained from the wavefront sensor is not sufficient, this beam dump could be replaced with a beam profiler package.

---

[1] A. Tribble, *Fundamentals of Contamination Control*, SPIE Press, 2000.

[2] P. Baumeister, *Optical Coating Technology*, SPIE Press, 2004.